Conserved Arginine Residues in Synaptotagmin 1 Regulate Fusion Pore Expansion Through Membrane Contact

Sarah B. Nyenhuis, Nakul Karandikar, Volker Kiessling, Alex Kreutzberger, Anusa Thapa, Binyong Liang, Lukas Tamm and David S. Cafiso*

From the Departments of Chemistry, Molecular Physiology and Biological Physics, and the Center for Membrane Biology, University of Virginia, Charlottesville, VA.

*Correspondence should be addressed to DSC, Department of Chemistry, McCormick Road, University of Virginia, Charlottesville, VA 22904; email: cafiso@virginia.edu, Tel: 434-924-3067.

Abstract

Synaptotagmin 1 is a vesicle-anchored membrane protein that functions as the Ca^{2+} sensor for synchronous neurotransmitter release. In this work, an arginine containing region in the second C2 domain of synaptotagmin 1 (C2B) is shown to control the expansion of the fusion pore and thereby the concentration of neurotransmitter released. This arginine apex, which is opposite the Ca^{2+} binding sites, interacts with membranes or membrane reconstituted SNAREs; however, only the membrane interactions occur under the conditions in which fusion takes place. Other regions of C2B influence the probably and kinetics of fusion but do not control the expansion of the fusion pore. These data indicate that the C2B domain has at least two distinct molecular roles in the fusion event, and the data are consistent with a novel model where the arginine apex of C2B positions the domain at the curved membrane surface of the expanding fusion pore.

Synchronous neurotransmitter release is a highly regulated process that results from the Ca^{2+}-triggered fusion of synaptic vesicles with the presynaptic plasma membrane. This fusion process is driven by the assembly of the three neuronal SNAREs (soluble N-ethylmaleimide sensitive receptor proteins), syntaxin (Syx) and SNAP-25 in the plasma membrane and synaptobrevin (Syb) in the vesicle membrane (1, 2). The assembly of the SNAREs into a four helical bundle or SNARE complex is highly favorable and provides the energy required to overcome the energetic barriers to fusion. Several other proteins interact with the SNAREs and are critical to the proper assembly of the complex, including Munc18, Munc13 and complexin (3). The Ca^{2+}-sensor for this process is the vesicle anchored protein, synaptotagmin 1 (Syt1), and the molecular event that initiates fusion is the binding of Ca^{2+} to the two C2 domains of Syt1 (4). However, the mechanism by which Ca^{2+} binding to the Syt1 C2 domains drives fusion is not understood.

The C2 domains of Syt1 are known to interact with and penetrate the membrane interface upon Ca^{2+} binding (5, 6). The second C2 (C2B) domain of Syt1 has a highly charged polybasic face that allows the domain to also associate in a Ca^{2+}-independent manner to negatively charged membrane interfaces (7). This interaction is weak to monovalent lipid such as phosphatidylserine (PS) but much stronger to membrane interfaces containing $PI(4,5)P_2$ (referred to here as PIP_2) (8). In the presence of Ca^{2+}, the Ca^{2+} binding loops and polybasic face work cooperatively to drive membrane association of the C2B domain. Synaptotagmin 1 is also known to associate with SNAREs, and several crystal structures have been generated showing the C2 domains of Syt1 in association with assembled SNAREs (9, 10). However, the interactions are heterogeneous, and they are not observed in the presence of ATP under conditions that resemble those found within the cell (11). Synaptotagmin 1 may trigger fusion by altering the local lipid bilayer structure, thereby stimulating a conformational change in the nearby SNARE complex catalyzing membrane fusion (12). There is also evidence that Syt1 might alter the vesicle membrane/plasma membrane distance, and conceivably this event might trigger SNARE assembly (13, 14). Synaptotagmin 1 also de-mixes PS upon membrane association (15), and this change in charged lipid distribution might modulate the membrane association of other proteins, such as Munc13 or the juxta-membrane regions of the SNAREs.

In addition to its charged polybasic face, the C2B domain of Syt1 has several highly conserved arginine residues in a region opposite the Ca^{2+}-binding loops that we will refer to as the arginine apex. Mutating this arginine apex is reported to dramatically depress evoked excitatory postsynaptic currents in hippocampal neurons, and this apex is proposed to allow the C2B domain to bridge across bilayers (16). There is also direct evidence that the arginine apex associates with lipid bilayers and that it could facilitate contact of the C2B domain with two opposing bilayers (17). In the present work, we demonstrate that the arginine apex is associated with the membrane when the C2B domain is membrane bound and that membrane contact is dependent upon conserved arginine residues in the domain. The arginine apex also associates with the SNAREs in a manner consistent with crystal structures. However, unlike the membrane interaction, the

interaction with the SNAREs is eliminated under conditions where fusion takes place. Using a single particle fusion assay with purified secretory granules, we find that the arginine apex does not affect the probability or kinetics of fusion but is necessary for the rapid release of secretory content, indicating that the apex has a role in controlling the expansion of the fusion pore. This result contrasts with that for the polybasic face, which alters the kinetics and probability of fusion but does not alter the rate of fusion pore expansion. The data indicate that there are two distinct molecular roles for Syt1 where different regions of the C2B domain make different contributions to the fusion process. We propose a novel mechanism for the action of Syt1 where the arginine apex of C2B helps position the domain at the negatively curved membrane surface that forms during the opening and expansion of the fusion pore.

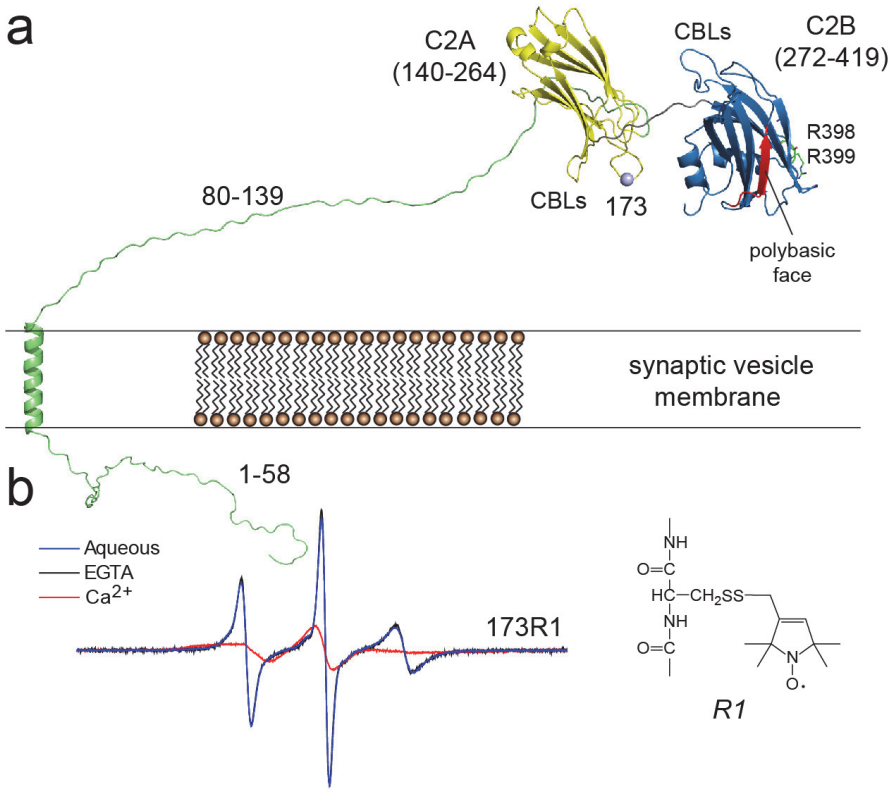

Figure 1. *EPR spectroscopy is sensitive to membrane proximity and insertion of labeled Syt1.* **a**) Model for Syt1 on the vesicle membrane surface showing position 173 in the 1st Ca^{2+}-binding loop (CBL) of the C2A domain (yellow). The position of the polybasic face (red) and R398, 399 side chains are shown for C2B (blue). **b**) EPR spectra from an R1 label attached to site 173. In the presence of Ca^{2+}, the domain inserts into the bilayer, which alters the sampling of rotamers by the R1 side chain and broadens the EPR spectrum.

Results

The arginine apex makes interactions with the membrane interface when Syt1 C2AB is membrane bound. Shown in Figure 1 is a model for Syt1 where the two C2 domains are attached to the vesicle membrane through a long linker. In the present work, we utilize a soluble fragment of Syt1 containing the C2A and C2B domains (residues 136-421). Site-directed spin labeling may be used to both monitor membrane contact and measure membrane depth, and our approach involves the incorporation of the spin labeled side chain R1 into selected sites in the protein. As shown in Figure 1b, membrane insertion of a region of the domain, in this case the first Ca^{2+}-binding loop of the C2A domain, produces a dramatic broadening in the EPR lineshape due to a reduction in the rotamers sampled by the R1 side chain.

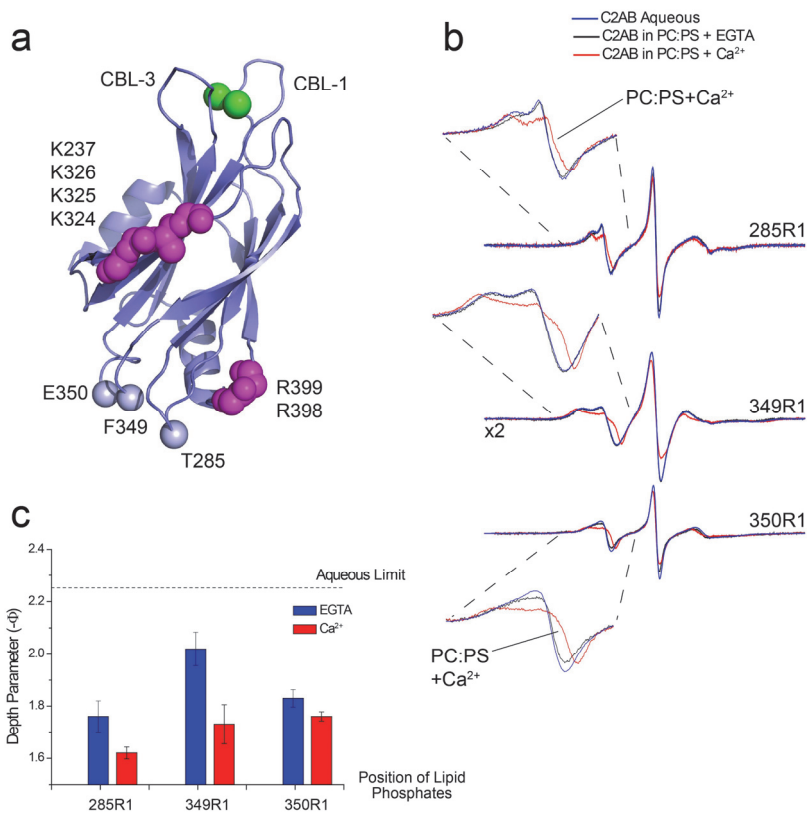

Figure 2. *The arginine apex of C2B contacts the membrane interface.* **a**) Model of C2B showing conserved arginine residues in the apex, lysine residues in the polybasic face and the three sites to which R1 was attached. The arginine apex is on the opposite surface of the domain from two Ca^{2+}-binding loops (CBL) that insert into bilayers in the presence of Ca^{2+}. **b**) EPR spectra from the three labeled sites in the absence of membranes or the presence of PC:PS lipid vesicles. **c**) Membrane depth parameters obtained with and without Ca^{2+} for labels near the apex.

To test for interactions in the arginine apex, spin labels were incorporated into three sites in the C2B domain that are depicted in Figure 2a, and the EPR spectra were recorded in the absence of membrane and in the presence of PC:PS vesicles with and without Ca^{2+}. When the C2B domain is membrane associated in the presence of Ca^{2+}, changes in the lineshapes from spin labels at sites 285, 349 and 350 are observed. The spectra show a slight broadening and a decrease in the residual hyperfine interaction, Azz', that may be due to the approach of the labels to the membrane interface. To confirm that these labels approach the membrane, progressive power saturation was used to provide an estimate of the distance of the labels to the membrane interface. As shown in Figure 2c, labels in the arginine apex lie close to the membrane interface in the presence of Ca^{2+} and are about 2

Angstroms from a plane defined by the lipid phosphates on the aqueous side of the membrane (Table S1, supplement). These three labels also tend to be near the interface in the absence of Ca^{2+}. This association may be facilitated by a weak association of the lysines forming the polybasic face of C2B (Figure 2a) to the PC:PS membrane interface. In the absence of Ca^{2+} and under the conditions of this measurement, there is likely a significant concentration of aqueous C2B domain that is in equilibrium with a population of membrane associated C2B.

When PIP_2 replaces PS in the membrane at equivalent charge densities, the EPR lineshapes and power saturation data also indicate that this region contacts the bilayer. As seen in Figure S1, site 350 makes a closer approach and site 285 is further away from the interface in PIP_2 than in PS. Interestingly, site 349 does not show strong evidence for contact, which likely reflects the altered orientation for the C2B domain when bound to a PIP_2 bilayer (8). The labeled position that shows the clearest evidence for membrane contact is site 350, and unlike the case for the interaction with PC:PS the interaction to PIP_2 does not appear to be Ca^{2+}-dependent. This likely reflects the enhanced Ca^{2+}-independent membrane affinity of C2B to the PIP_2 bilayer relative to the bilayer containing PS (8). Thus, we conclude that when C2AB is attached to the membrane interface, the arginine apex is also in contact with the bilayer surface.

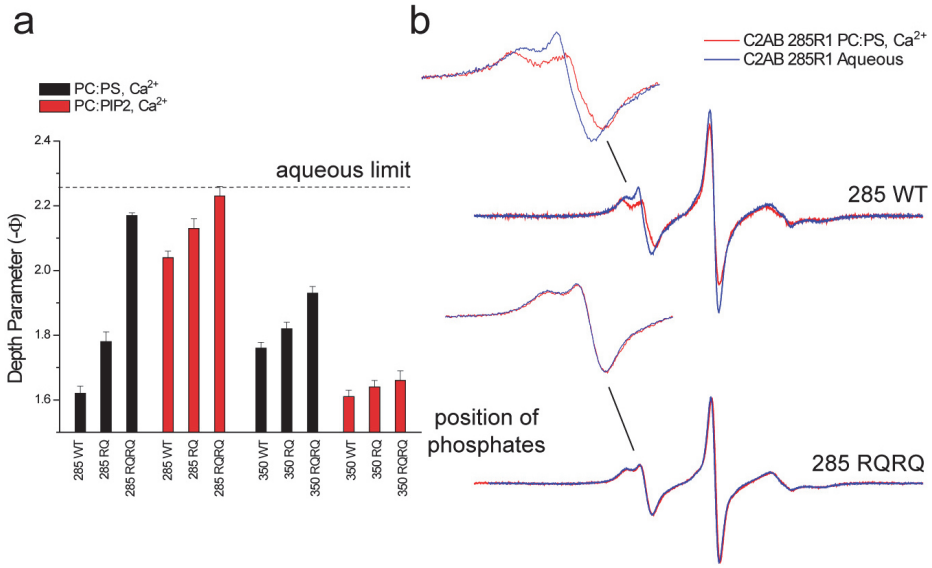

Figure 3. *Mutating the arginine apex reduces or eliminates membrane contact by the arginine apex*. **a**) power saturation indicates that the RQ and RQRQ mutations reduce or eliminate membrane contact. **b**) EPR spectra obtained from site 285 for the pseudo wild-type (WT) and RQRQ mutant. EPR spectra are identical in the absence or presence of membranes for the RQRQ mutant. A depth parameter of 2 is obtained for an R1 label that lies approximately 4 Å from the lipid phosphate. When the labeled is further than 6 or 7 Å from the phosphates, the depth parameter becomes independent of label position.

Membrane contact at the apex is driven by conserved arginine residues. We then examined the effect of two sets of mutants, R398Q (RQ) and R398Q/R399Q (RQRQ) on the membrane depth

parameters from the two most closely associating positions, 285 and 350, on the C2B domain of Syt1. Figure 3a shows the results of power saturation measurements for the wild-type C2AB versus the single RQ and double RQRQ mutations (Table S2, supplement). Each arginine mutation shifts the apex further towards the aqueous phase or eliminates the membrane interaction, with the double RQRQ mutation showing the largest effects. For example, in the presence of PC:PS the RQRQ mutation shifts the position of 285R1 approximately 5 Å towards the aqueous phase. In PC:PIP_2, the RQRQ mutation eliminates the membrane interaction of 285R1. Shown in Figure 3b are comparisons of the EPR spectra from site 285 with and without membrane for the wild-type C2AB and RQRQ mutation. The spectra obtained from site 285 in the presence of the RQRQ mutation are identical with and without membrane indicating that there is no membrane contact at this site in the presence of the RQRQ mutation.

The arginine apex contacts membrane reconstituted SNARE proteins. The arginine apex has been observed to interact with the soluble SNARE complex by x-ray crystallography (9). We also examined the EPR spectra from the three spin labeled sites at the apex of C2B to test for this interaction with SNARE complexes embedded in lipid bilayers. Shown in Figure 4a are EPR spectra from sites 285, 349 and 350 in the presence of PC:PS membranes with or without membrane reconstituted SNAREs composed of full-length Syx, SNAP-25, and soluble Syb. The spectra for sites 285 and 350 have reduced normalized amplitudes and broadened hyperfine extrema (Azz') indicating that the motion and rotamer sampling of the nitroxide at these sites is being sterically restrained by interactions with the SNAREs. We examined the rotamers available at these sites as predicted from the crystal structure (PBD ID: 5CCH) using the program MMM (18) and the result is shown in Figure 4b. According to this model, the R1 label at all three sites should contact the SNAREs, with sites 350 and 285 having the greatest reduction in the available rotamers and site 349, which projects away from the SNAREs, having the least. This is consistent with the data in Figure 4a and indicates that these EPR data in the presence of membrane reconstituted SNAREs is consistent with the model from crystallography.

The addition of ATP or the presence of PIP_2 in the membrane eliminates the SNARE interactions but does not eliminate the membrane interactions of the arginine apex.
Next, we tested the effect of the RQ mutations and mutations in SNAP-25 on the association of Syt1 with the SNAREs. Interactions between Syt1C2AB and the SNAREs are likely driven by charge interactions, and we mutated three negatively charged residues D51, E52 and E55 to alanine in the N-terminal segment of SNAP-25. As seen in Figure 4c, a comparison of the EPR spectra from spin labeled sites in the Syt1C2AB arginine apex show no differences between PC:PS membranes alone and PC:PS membranes containing SNAREs with this AAA mutant. The result indicates that the AAA mutation eliminates the Syt1C2AB-SNARE interaction. Importantly, as shown below, this mutation somewhat reduces docking of secretory vesicles and their overall fusion, but it does not alter the Ca^{2+} dependent release mode (fusion pore opening) and Ca^{2+} stimulated fusion increase. Figure 4d compares normalized amplitudes of spectra obtained from

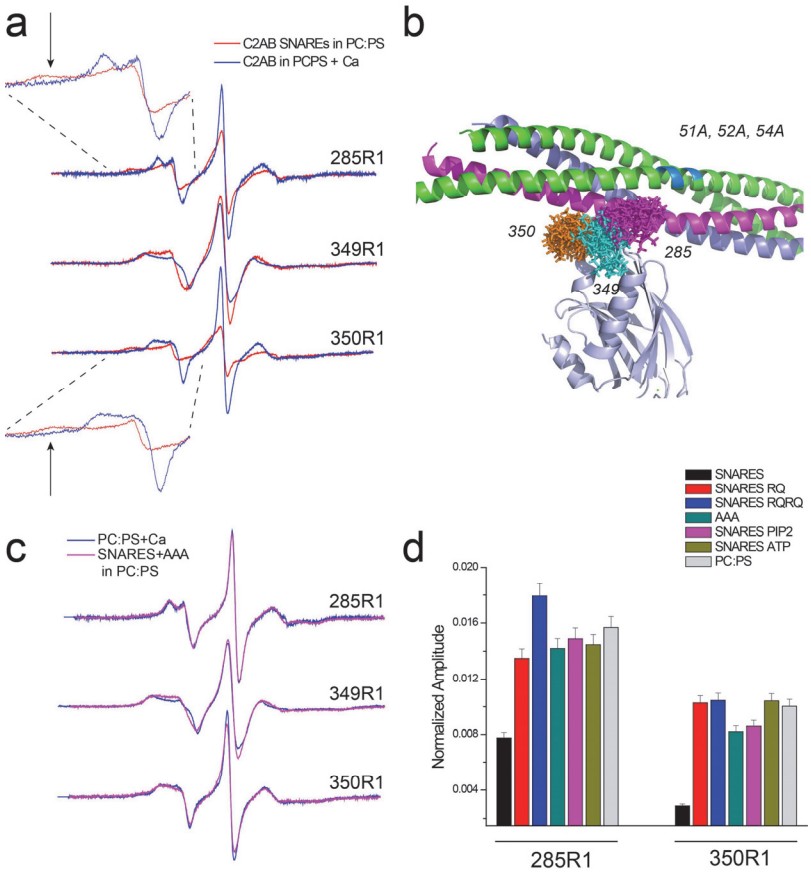

Figure 4. *The arginine apex contacts membrane reconstituted SNAREs, but ATP or PIP_2 in the bilayer, eliminate the interaction.* **a**) EPR spectra in the absence (blue trace) or presence (red trace) of membrane reconstituted SNARE complex composed of full-length Syx, SNAP-25, and soluble Syb. The broadened components of the hyperfine tensor (arrows) indicate tertiary contact of the R1 side chain with SNAREs. **b**) Model (PDB ID 5CCH) with available rotamers for the R1 side chains at the three sites. **c**) Comparison of EPR spectra with and without membrane reconstituted SNAREs containing the AAA mutation in SNAP-25. **d**) Normalized amplitudes for EPR spectra from sites 285R1 and 350R1. Larger amplitudes indicate loss of tertiary contact with the SNAREs.

285R1 and 350R1 in the presence of membrane reconstituted SNAREs, membrane reconstituted SNAREs having the AAA mutation, as well as membrane reconstituted SNAREs in the presence of the RQ and RQRQ mutations. Both single and double RQ mutations, as well as the AAA mutation, yield normalized amplitudes like those obtained for membranes lacking the SNAREs (composed only of PC:PS), indicating that the Syt1/SNARE interaction no longer takes place. The addition of 1 mM ATP/Mg^{2+} (a typical cytoplasmic concentration) also eliminates interactions between C2AB and the membrane reconstituted SNAREs as does the presence of 5 mol% PIP_2 in the membrane (Figure 4d).

As seen in Figures 3 and 4, both the membrane and SNARE interactions of the arginine apex are sensitive to the RQ and RQRQ mutations. Thus, both interactions require these conserved arginine residues and are likely driven by electrostatics. However, the SNARE interaction is eliminated by PIP_2, whereas the membrane interaction is not. SNARE interactions are also eliminated by ATP, which is also not the case for the membrane interaction (see Figure S2).

Mutations in the arginine apex do not alter fusion probability but alter the rate of fusion pore opening. The data in Figures 3 and 4 indicate that conserved arginine residues in the apex of the C2B domain facilitate membrane contact of the apex under the conditions where fusion takes place. To better define their role in the fusion process, we used a single particle fusion assay to examine fusion between chromaffin secretory granules purified from PC12 cells (also referred to as dense core vesicles, DCVs) and reconstituted planar supported membranes containing recombinant syntaxin-1a and dSNAP-25 (dodecylated SNAP-25). These purified chromaffin granules were previously shown to be composed of the same molecular machinery as synaptic vesicles purified from rat brain (19). An important feature of this assay when investigating the machinery of secretion is the ease of engineering stable knockdowns into PC12 cells and thus producing cell-derived vesicles with syt1 depletions and no other changes.

The chromaffin granules are labeled by expressing the releasable content marker neuropeptide Y (NPY)-mRuby, and their binding to planar supported membranes in a SNARE dependent manner (schematic in Figure 5a, left) can be observed using total internal reflection fluorescence microcopy (TIRFM) (20). Granule binding is accompanied by an increase in fluorescence within the TIRF field, where a subset of the granules fuse after a variable time delay (Fig. 5b). Fusion is marked by a decrease in fluorescence followed by a rapid spike in fluorescence signal and then a further decay in signal (Fig. 5b and c). The initial decay in the signal is caused by the loss of NPY-mRuby from the granule as it diffuses into the cleft between the supported membrane and its supporting slide during an initial slow release phase. The rapid increase in fluorescence is a result of the rapid collapse of the granule as fluorescent marker is rapidly driven into the evanescent field of the TIRFM. As NPY-mRuby continues to diffuse away from the fusion site, the signal decays. The origin of this signal has been previously described in detail (19, 20) and is modulated by the lipid geometries that stabilize or destabilize fusion pores (21).

When granules are depleted of endogenous synaptotagmin isoforms, Ca^{2+}-dependent fusion is lost; however, addition of the soluble C2AB domain recovers the Ca^{2+} dependence (Fig. 5d). The intensity of the spike in fluorescence (ΔI_C) is indicative of the amount of content released from the granule during the fast phase of the fusion event after the initial slow release. The value of ΔI_C reflects the mode of contents release, or the timing of the fusion event, and in our model it is

dependent upon the speed with which the granules transition between the initial slow and fast phases of contents release. As seen in Figure 5c, this release mode is modulated by the presence of C2AB and 100 μM Ca^{2+} when granules depleted of endogenous synaptotagmin are used. The C2AB domain was previously shown to catalyze a structural transition in the SNARE complex by interactions mediated through the membrane bilayer (12). This structural transition involves a change in SNARE orientation relative to the membrane, i.e. a transition from a trans-mimicking conformation to a cis-mimicking conformation, which can be monitored using site directed fluorescence interference contrast microscopy (sdFLIC) (Figure 5a, right) (12). As seen in Figure 5e this conformational change is dependent on C2AB and calcium. Combining the TIRF fusion and sdFLIC assays creates a powerful tool to examine secretory granule binding, fusion probability, content release, SNARE complex conformational changes, and kinetics of fusion, all under the same conditions. In the context of the various Syt1 mutations and their modulated interactions with membranes and SNAREs, this approach allows us to tease out the role of Syt1 in fusion.

Figure 5f shows the effects of three sets of mutants in C2B on granule binding, fusion efficiency, content release, structural changes in the SNAREs, and kinetics of fusion. Here, we examined a single arginine mutation in the apex (RQ), mutation of both arginines in the apex (RQRQ), or lysine mutations in the polybasic face (KAKA). In the absence of Ca^{2+}, granule binding is mediated by SNAREs, and in the presence of Ca^{2+} it is mediated by both SNAREs and the vesicle-resident calcium binding protein CAPS (20). Figure 5f shows that these mutations in C2B have no effect on granule binding. When the percentage of granule fusion events is examined, only mutations in the polybasic face (KAKA) depress the fusion efficiency, while mutations in the arginine apex have no effect. However, when we examine the timing of the fusion event (the release mode), the KAKA mutant has no effect while mutations in the arginine apex strongly affect the release mode. Thus, mutations in the apex strongly affect the transition from the slow to fast phase of content release, i.e. the transition from the opening to the dilation of the fusion pore. In contrast, as shown previously (12), mutations in the arginine apex produce only small perturbations in the conformation change of SNARE complex (measured by sdFLIC) compared to wild-type C2AB, while stronger effects on this orientational change are observed for the KAKA mutation. The polybasic face also had a greater effect on the kinetics of the delay time from granule binding to fusion, while the arginine apex mutations had only a slight effect.

As seen in Figure 5f, the SNARE structural changes strongly correlate with the fusion efficiency and kinetics, and it is interesting to note that the effects of these C2B mutants track with their effect on C2AB membrane affinity. The KAKA mutant, which had the largest effect on SNARE structural changes and fusion, is known to reduce the membrane affinity of C2AB in the presence of PIP_2 (8). In contrast, the membrane affinity of C2AB was measured for the RQRQ mutation in the apex and was found to produce no significant change in affinity (see Figure S3). The data in Figure 5f indicate that the membrane binding of Syt1 C2AB is necessary to initiate fusion, but that

the membrane interactions made by the arginine apex are required to for the proper timing of the fusion event and the rapid opening of the fusion pore.

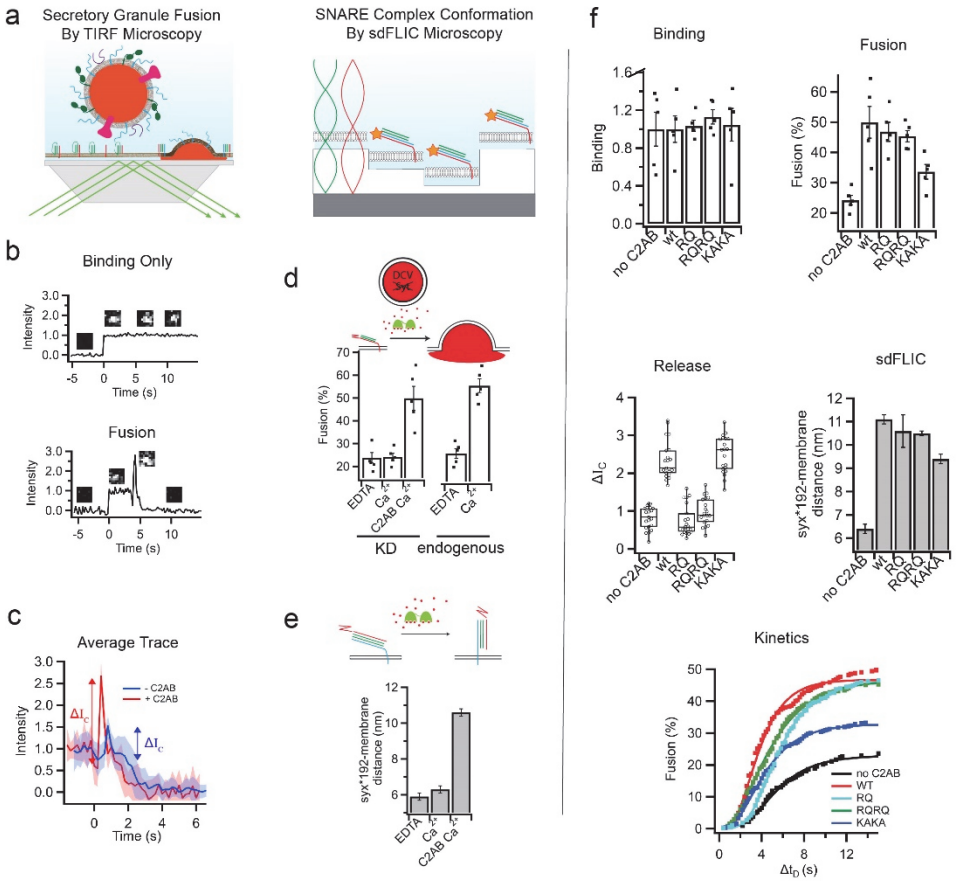

Figure 5. *The effects of synaptotagmin mutations in C2B on secretory granule fusion and SNARE orientation.* **a**) Single granule supported membrane TIRF fusion assay (left) and sdFLIC microscopy of the ternary SNARE complex (right). **b**) Fluorescence intensity traces of single granules interacting with supported membranes in a TIRF microscope. After a sudden increase in fluorescence, indicating binding, the intensity stays constant if the granule never fuses (top) or the trace shows a characteristic dip and peak after different delay times (bottom) if the granule membrane fuses with the reconstituted supported membrane. **c**) Averaged traces (20 events per trace) showing a fast mode of fusion in the presence of C2AB (red) or slow mode of fusion in the absence of C2AB (blue). Both conditions were in the presence of 100 μM Ca^{2+}. **d**) Granules depleted of synaptotagmins (Syt1 and Syt9) do not fuse in response to calcium. 0.4 μM soluble C2AB stimulates fusion of synaptotagmin knock down granules to a similar level as granules containing endogenous synaptotagmin in the presence of 100 μM Ca^{2+} (membrane composition was 32:32:15:20:1 bPC:bPE:bPS: Chol:PI(4,5)P_2). **e**) Structural changes in the orientation of the ternary SNARE complex in the presence of calcium and 0.4 μM C2AB. **f**) The effects of RQ, RQRQ, or KAKA mutations in C2AB on granule binding, fusion, release characteristics, SNARE orientation, and fusion kinetics in the presence of 100 μM Ca^{2+} (membrane composition was 32:32:15:20:1 bPC:bPE:bPS:Chol:PI(4,5)P_2).

The C2B domain makes simultaneous membrane contact at the arginine apex, the polybasic face and the Ca^{2+}-binding loops. The data shown in Figure 2 indicate that the arginine apex

contacts negatively charged membranes whenever the C2B domain is membrane associated. However, other regions of C2B also make membrane contact. In the presence of PIP_2 and under the same conditions that attach the arginine apex, the Ca^{2+}-binding loops penetrate and the polybasic face interacts with PIP_2 (8). These interactions are evident in the EPR spectra shown in Figure 6a, where the EPR spectra and power saturation data show that these regions of C2B are interacting with the membrane interface and with PIP_2 (Figure 6b and Table S3).

Inspection of the spectra from sites 304 and 329 indicates that for virtually the entire population of C2B, these regions are membrane associated or interacting with PIP_2. Multiple components in the spectra that would indicate an equilibrium between aqueous and membrane associated C2B are not seen. Such an equilibrium would be more difficult to distinguish in the spectra from the apex (Figure 2), where spectra corresponding to bound and unbound apex are similar. Nonetheless, the presence of a mixture of membrane associated and aqueous states is not obvious. Thus, a large fraction of C2B must undergo simultaneous membrane contact at these sites. Shown in Figure 6c are the allowable rotamers of the nitroxide spin label at each of the membrane interacting sites. It is not possible to simultaneously satisfy these interactions with a flat planar bilayer interface or two parallel bilayer surfaces; however, these interactions can be satisfied if the C2B domain interacts with a curved membrane interface.

Removal of PIP_2 alters granule binding, fusion, fusion pore opening, and SNARE conformational changes. The association of the polybasic face with the membrane interface seen in Figure 6a is driven by PIP_2, and we tested the effect of PIP_2 on granule fusion and SNARE conformation as described above for the C2B mutants. As shown in Figure 6d, removal of PIP_2 in the presence of 100 μM Ca^{2+} reduces granule binding, fusion efficiency, slows the fusion timing or release mode, alters SNARE conformation, and reduces fusion kinetics. The loss of PIP_2 will reduce C2AB affinity and should have a similar effect as the KAKA mutant. But the loss of PIP_2 also produces an effect on the opening of the fusion pore that is similar to that of the RQ and RQRQ mutants (Figure 5f). The change in calcium stimulated granule binding mediated by PIP_2 was previously demonstrated to be dependent on CAPS which is a membrane associated calcium binding protein with a PIP_2 specific PH domain (20).

The SNAP-25 AAA mutation has no effect on granule contents release and the opening of the fusion pore. As shown above in Figures 4c, d, mutation of SNAP-25 to replace three negatively charged residues (the SNAP-25 AAA mutation) eliminated the SNARE binding of the arginine apex. We tested to see what effect these mutations would have on the granule docking and fusion and the opening of the fusion pore. As seen in Figure 6e, in the presence of Ca^{2+} the AAA mutation reduces, but does not eliminate, granule binding and fusion efficiency. However, the effects of the AAA mutation are also seen in the absence of Ca^{2+} or C2AB, indicating that they are not mediated by C2AB. In contrast to the RQ and RQRQ mutations (Figure 5f), the AAA mutation has no effect on the release mode or timing of the fusion event. Since this mutation eliminates the

SNARE interactions made by the C2B arginine apex, SNARE interactions of the apex are not necessary to mediate changes in Ca^{2+}-dependent fusion pore opening.

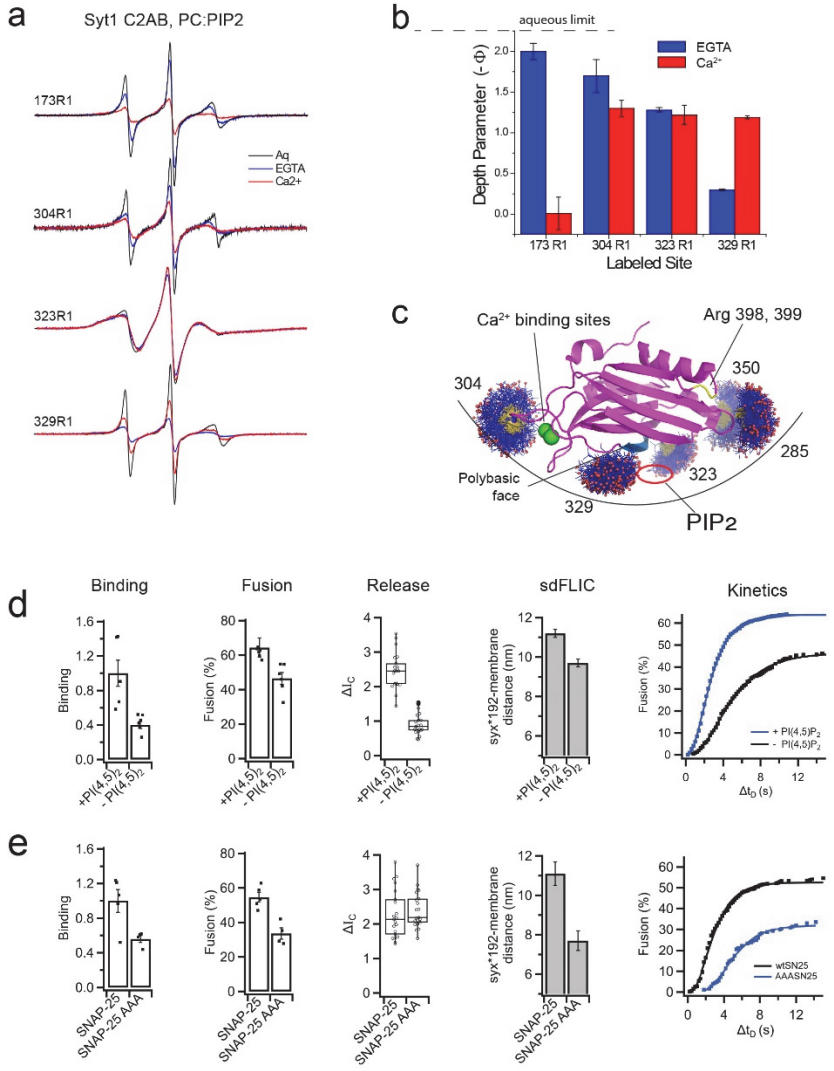

Figure 6. *The C2B domains makes simultaneous membrane contact at multiple sites that cannot be explained by docking to a planar bilayer surface.* **a**) EPR spectra in an aqueous state compared with spectra in the presence of PC:PIP_2 bilayers in the presence of EGTA or Ca^{2+}. **b**) Membrane depth parameters indicate that site 173 inserts into the PIP_2 bilayer in the presence of Ca^{2+}. Sites on C2B including 304, 323 and 329 also contact with bilayer, with or without Ca^{2+}. **c**) Allowable rotamers for labeled sites that contact the membrane interface including two near the arginine apex. The membrane contact seen at these sites could be accommodated by a curved membrane surface. This would place a PIP_2 headgroup in a binding pocket at the polybasic face. d) The effect of $PI(4,5)P_2$ on granule binding, fusion, release profile, SNARE orientation, and fusion kinetics in the presence of 100 μM Ca^{2+} (membrane composition was 25:25:15:30 bPC:bPE:bPS:Chol and either 5% PI or 4% PI with 1% $PI(4,5)P_2$). **e**) The effect of the AAA mutation in SNAP-25 on granule binding, fusion, release profile, SNARE orientation, and fusion kinetics in the presence of 100 μM Ca^{2+} (membrane composition 32:32:15:20:1 bPC:bPE:bPS:Chol:$PI(4,5)P_2$).

Discussion

Despite its central importance for synchronous neurotransmitter release, the molecular mechanisms underlying Syt1 function are presently unclear. Molecular models for Syt1 in association with SNAREs have been generated by X-ray crystallography, and they suggest that the Ca^{2+} regulatory event involves a control of the SNAREs by a direct interaction with Syt1 (9, 10). However, other data indicate that the interactions of Syt1 with SNAREs are weak, heterogeneous, and are of secondary importance to the interactions made by Syt1 to membranes (11).

In the present work, we examined a region on the C2B domain that lies opposite the Ca^{2+}-binding loops that contains a pair of conserved arginine residues at sites 398 and 399. Mutating this pair of residues to glutamine (RQRQ mutation) is known to have a significant effect on synchronous neurotransmitter release and excitatory postsynaptic potentials (16), and our initial goal was to determine whether the effect of these mutations was acting at the level of a membrane or direct SNARE interaction. As shown in Figures 2 and S1, the arginine apex associates with membranes whenever Syt1 C2AB is membrane associated. The apex also associates with membrane reconstituted SNAREs in a manner that is consistent with molecular structures generated by crystallography, and both membrane and SNARE interactions are weakened or eliminated by the RQ and RQRQ mutations. However, the data presented here indicate that only the membrane interactions of the C2B apex occur under conditions where fusion takes place.

The interaction made by the arginine apex with membrane reconstituted SNAREs is eliminated when PIP_2 is present in the membrane (Figure 4d), or when ionic conditions mimic those expected within the cell. In addition, mutation of three basic residues within SNAP25 (the AAA mutation) also eliminates the Syt1-SNARE interaction (Figures 4c, d). However, the AAA mutation does not abolish membrane docking or fusion (Figure 6e), and it has no effect on the rate of fusion pore expansion during the fusion event, indicating that interactions between the C2B arginine apex and SNAREs are not involved in Ca^{2+}-triggered neuropeptide release. In contrast, when PIP_2 is present in the membrane, the apex of C2B contacts membranes under all conditions we examined and is progressively weakened by the RQ and RQRQ mutations. These mutations in the apex have a profound effect on the rate at which the fusion pore opens and the concentration of vesicle content that is released quickly into the TIRF field (Figure 5f). These data demonstrate that the membrane interactions of the apex of Syt1, and not the SNARE interactions, regulate the fusion pore expansion.

Previous work has shown that Syt1 C2AB binds preferentially to membranes rather than SNAREs when PIP_2 is present, an interaction that is mediated by the polybasic face of C2B (8, 11). Here, the KAKA mutation in the polybasic face of C2B did not alter the opening of the fusion pore (Figure 5f), rather it altered SNARE conformational changes and fusion probability and kinetics. The result indicates that the apex plays a role in Syt1 function that is distinct from that of the

polybasic face and that there are at least two molecular roles played by C2B that are important for fusion.

Isoforms of synaptotagmin are known to have different behaviors with respect to Ca^{2+}-sensitivity and synchronous release (22). The arginine apex appears to be important in controlling the release mode of synaptotagmins, as shown by a comparison of the behavior of the Syt1 RQ and RQRQ mutants with that of synaptotagmin-7 (Syt7). Using the same single particle fusion assay as that used here, Syt7 demonstrates a substantially lower release rate than does WT Syt1 (23); however, the rates of release for Syt7 are similar to those seen here for either the RQ or RQRQ mutations of Syt1 (Figure 5f). A comparison of the sequence of the arginine apex for Syt1 and Syt7 shows that Syt7 is RQ rather than RR, and thus is identical in this regard to the Syt1 RQ mutant. We speculate that Syt7 and the RQ mutant of Syt1 look similar in terms of the rate of fusion pore opening because both proteins have the same residues in this apex.

How might membrane interactions of the apex of C2B act to mediate membrane fusion and alter the characteristics of the fusion pore? In previous work, membrane interactions made both by the arginine apex and the Ca^{2+}-binding loops on opposite surfaces of the domain suggested a model where C2B bridged across two parallel bilayer planes, perhaps ultimately functioning to shorten the vesicle-plasma membrane distance in the presence of Ca^{2+} (14, 17). However, the data presented here indicate that in the presence of PIP_2, the polybasic face also contacts the PIP_2 headgroup (Figure 6a,b), so that three regions of the C2B domain make membrane contact. The EPR lineshapes indicate that the interaction of the polybasic face and the Ca^{2+}-binding loops are stable interactions that are not transient. This is more difficult to determine for the arginine apex, but nonetheless simultaneous membrane interactions of each of these three regions must occur for at least some period. It is not possible to dock the C2B domain to either one planar bilayer surface or to two parallel planar bilayer surfaces so that contact in all three regions is satisfied. But simultaneous interactions in all three regions of C2B can be satisfied if the domain is interacting with a curved bilayer interface (Figure 6c). Indeed, recent simulations suggest that mixtures of lipids likely to mediate fusion can form punctate surfaces with regions of negative curvature (24), which might accommodate this type membrane interaction of C2B.

Shown in Figure 7 is a model for the membrane interactions made by Syt1 that incorporates what is known about the molecular interactions made by C2B and the effect of mutations in the arginine apex on granule binding and fusion. In this model, Syt1 is interacting at the negatively curved surface that is present following the formation of a hemifusion intermediate. As the fusion pore forms, the C2B domain of Syt1 interacts with this negatively curved surface making contact at the Ca^{2+}-binding loops, arginine apex and polybasic face. In doing so, the C2B domain of Syt1 helps mediate the transition during a fusion event to a fully open pore. It might mediate this transition by either lowering an energy barrier for pore expansion or by preventing the system from getting trapped at an early intermediate state during the pore opening (25). By weakening or eliminating

membrane contact at the apex with either the RQ or RQRQ mutations, the C2B domain no longer assumes the correct orientation across the cytoplasmic side of the fusion pore, and the mode of contents release or progression to a fully open fusion pore is slowed (Figure 5f). Other than the RQ and RQRQ mutations, PIP_2 is the other component that is seen to strongly influence the release mode or pore opening when it is removed (Figure 6e). Interestingly, the polybasic face is aligned facing into a region of high negative curvature in this model. Since it interacts with PIP_2, this lipid would be driven into an interface of negative curvature. PIP_2 is a lipid that alone will tend to form micelles (26, 27), and its position within the negative curve of the growing fusion pore would not be energetically favored. Conceivably, the presence of PIP_2 in this region of the pore, driven by strong electrostatic interactions with the polybasic face of C2B, might act to destabilize an initial state in the fusion pore and drive it to a fully open state.

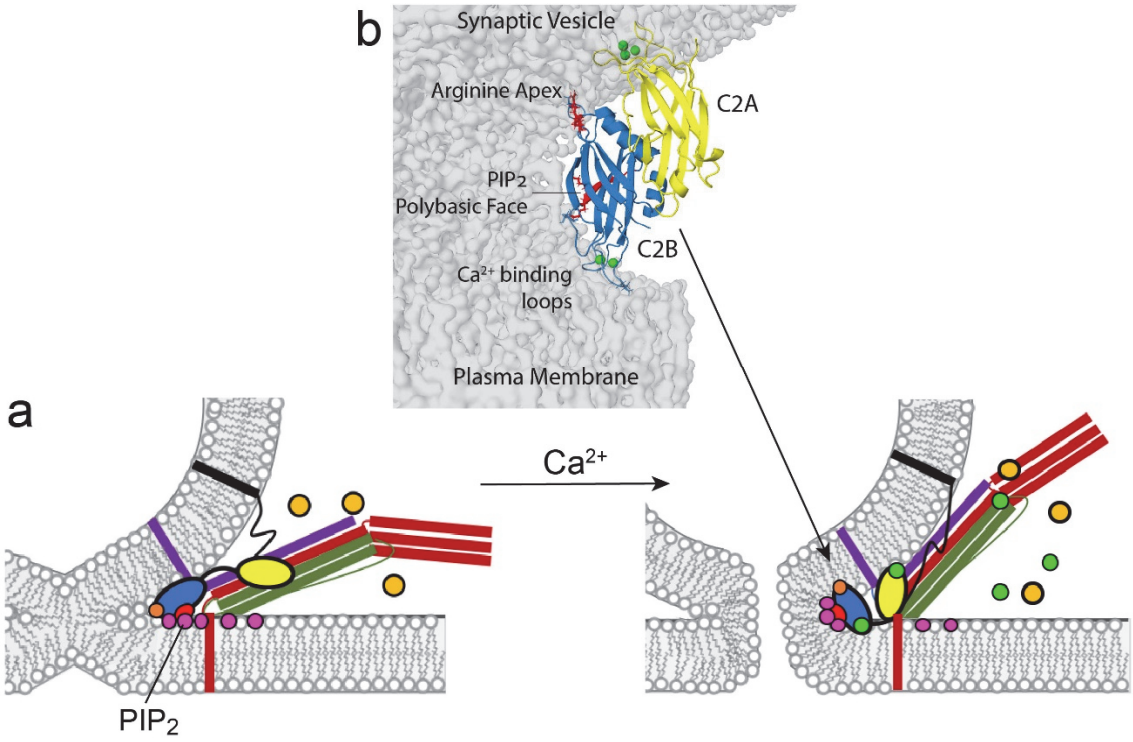

Figure 7. In (**a**) after docking to the bilayer and in the presence of ATP/Mg^{2+} (orange) the SNARE complex, syntaxin (red), SNAP-25 (green), synaptobrevin (purple), and Syt1 C2B (blue), promote partial lipid mixing by either zippering or contacting plasma membrane PIP_2 at the arginine apex (orange) and the polybasic face (red). Upon calcium influx (green), Syt1 C2A inserts into the synaptic vesicle membrane, PS, and C2B reorients, binding the Ca^{2+}-binding loops at a 3rd membrane contact point. The C2B domain of Syt1 might position at the site of fusion as shown in (**b**). This orientation would sequester PIP_2 into the strained membrane stalk, further destabilizing the membrane and promoting pore opening.

In summary, the data presented here are consistent with a novel model for the role of Syt1 where the C2B domain interacts with the negatively curved membrane surface during the initial stages of fusion to mediate expansion of the fusion pore. Using both EPR spectroscopy and single particle

fusion experiments we demonstrate that the arginine apex of C2B helps control the opening or dilation of the fusion pore and mediate the transition between the initial pore opening and a fully open fusion pore. We demonstrate that the C2B domain interacts both with membranes and membrane associated SNAREs; however, only the membrane interaction takes place under the conditions where fusion occurs. As a result, the expansion of the fusion pore is mediated by a membrane interaction of the C2B arginine apex. Mutations that lie in the polybasic face of C2B alter the fusion probability but have no effect on the expansion of the fusion pore once fusion occurs, indicating that there are at least two molecular roles for Syt1 in triggering fusion.

Methods

Expression and purification of Syt1 and SNAREs proteins

Expression and purification of C2AB (residues 136–421) from *Rattus norvegicus* was carried out as previously published (8, 14). The native cysteine at residue 277 was mutated to an alanine, and C2AB was expressed using a pGEX-KG construct with an N-terminal GST tag. For electron paramagnetic resonance (EPR) measurements the single site of interest was mutated to a cysteine using Polymerase Incomplete Primer Extension (PIPE) site-directed mutagenesis in order to attach a spin label at sites: M173C, T285C, V304C, L323C, T329C, F349C, and E350C. For neutralization of the arginine apex, R398Q (RQ) or R398QR399Q (RQRQ) were also introduced to the cys-free construct, the T285C plasmid, and the E350C plasmid. For EPR experiments, expression, and purification of the SNARE complex, derived from *Rattus norvegicus,* was carried out as described previously, using N terminal His6-tags (28)**.** The complex was composed of full-length cysteine free syntaxin, full-length cysteine free SNAP25A, where all 4 cysteines were replaced by serine, and soluble synaptobrevin (residues 1-96). For the AAA mutant SNARE complex, cysless-SNAP25A was substituted for an additional triple alanine mutation at the negatively charged positions: D51, E52, E55. DNA sequencing for all mutations were verified by GENEWIZ DNA sequencing (South Plainfield, NJ).

SNARE complex assembly

For SNARE complex assembly, purified individual components of SNARE proteins were mixed in the molar ratio of 1:1:1 in assembly buffer (20mM HEPES, pH7, 150mM NaCl, 1mM EDTA) with the presence of 0.1% DPC. Usually SNAP25 and synaptobrevin were mixed first in buffers without DPC, after raising DPC concentration to 0.1%, according amount of syntaxin were added for overnight incubation at 4°C. The reaction mixture was then purified with ion-exchange chromatography (MonoQ) to remove small amounts of unreacted monomers.

Continuous wave EPR

Experiments were performed as described previously using a Bruker X-Band EMX spectrometer (Bruker BioSpin, Billerica, MA) equipped with an ER 4123D dielectric resonator (1, 3). All EPR spectra were recorded at room temperature with 100-G magnetic field sweep, 1-G modulation, and 2.0-mW incident microwave power. The CW measurements were performed on 4 to 6-μL samples in glass capillary tubes (0.60 mm inner diameter × 0.84 mm outer diameter round capillary; VitroCom, Mountain Lakes, NJ). The phasing, normalization, and subtraction of EPR spectra were performed using in-lab software written by David Nyenhuis. To assess the membrane binding, ~50-100 μM of spin-labeled C2AB was added to either charged LUVs at a 1:200 protein:lipid ratio (~10-20 mM concentration) of POPC/POPS (80:20) or POPC/PIP_2 (95:5)). To assess membrane and SNARE binding, cys free or AAA SNAREs were reconstituted at a 1:400 protein:lipid ratio of the same lipid compositions by dialysis in the presence of Bio-Beads (Bio-Rad Laboratories, Hercules, CA) into metal-free buffer. C2AB was added to proteoliposomes containing SNAREs

at a 1:1:200 C2AB:SNAREs:lipid ratio. The EPR spectra were recorded in the presence of 1 mM Ca^{2+}, after the addition 1mM ATP/Mg^{2+}, and after the addition of 4 mM EGTA. Progressive Power saturation of the EPR spectra was performed as described previously (8). Briefly, samples were placed in gas-permeable TPX-2 capillaries. Then each sample was run in the presence of air (O_2) or Ni(II)EDDA to determine the membrane depth parameter, Φ. The spin label depth was estimated using the following expression: $\Phi = A[tanh(B(x - C)) + D]$, where x is the distance of the spin label from the phospholipid phosphate plane in the bilayer, and A, B, C, and D are empirically determined constants (29).

Fluorescent labeling

His-tagged syntaxin-1a was reacted with an at least twofold molar excess of Alexa-546 in thoroughly degassed DPC-buffers. Labeled proteins were separated from free dye via extensive wash after re-binding to Ni-NTA column. Subsequently, eluted Alexa-labeled proteins were subjected to thrombin cleavage and then purified by size-exclusion chromatography (30).

Reconstitution of SNAREs into proteoliposomes

All SNARE proteins, acceptor complex and SNARE complexes, were reconstituted using sodium cholate as previously described (31). The desired lipids (composition as indicated in Figure legend) were mixed, and organic solvents were evaporated under a stream of N_2 gas followed by vacuum desiccation for at least 1 hour. The dried lipid films were dissolved in 25 mM sodium cholate in buffer (20 mM HEPES, 150 mM KCl, pH 7.4) followed by the addition of an appropriate volume of the desired SNARE protein(s) (syx/dSNAP25 for fusion experiments and syx*192/SNAP25/syb1-96 for sdFLIC experiments) in their respective detergents to reach a final lipid/protein ratio of 4000 (sdFLIC and SytKD-DCV fusion) or 3000 (wt DCV fusion) for each protein. After 1 hour of equilibration at room temperature, the mixture was diluted to reach a sodium cholate concentration of 16 mM, close to the critical micellar concentration, by adding more buffer to the desired final volume. The sample was then dialyzed overnight against 1 L of buffer with 1 buffer change after ~4 hours.

Preparation of planar supported bilayers containing SNARE complexes

Planar supported bilayers with reconstituted plasma membrane SNAREs were prepared by the Langmuir-Blodgett/vesicle fusion technique as described in previous studies (32-34). FLIC chips or quartz slides were cleaned by dipping in 3:1 sulfuric acid: hydrogen peroxide for 15 minutes using a Teflon holder. Slides were then rinsed thoroughly in Milli-Q water. The first leaflet of the bilayer was prepared by Langumir-Blodgett transfer directly onto the quartz slide using a Nima 611 Langmuir-Blodgett trough (Nima, Conventry, UK) by applying the lipid mixture of 80:20:3 bPC:Chol:DPS for experiments with SytKD DCVs or 70:30:3 bPC:Chol:DPS for experiments with wt DCVs from a chloroform solution. After allowing the solvent to evaporate for 10 minutes, the monolayer was compressed at a rate of 10 cm^2/minute to reach a surface pressure of 32 mN/m. After equilibration for 5 to 10 minutes, a clean quartz slide was rapidly (68 mm/minute) dipped into the trough and slowly (5 mm/minute) withdrawn, while a computer maintained a constant

surface pressure and monitored the transfer of lipids with head groups down onto the hydrophilic substrate. Proteoliposomes were incubated with the Langmuir-Blodgett monolayer to form the outer leaflet of the planar supported bilayer. A concentration of 77 mM total lipid in 1.2 mL total volume was used. After incubation of the proteoliposomes for 2 hours the excess proteoliposomes were removed by perfusion with 10 mL of buffer (120 mM potassium glutamate, 20 mM potassium acetate, 20 mM HEPES, pH 7.4 for DCV fusion experiments or 150 mM KCl, 20mM HEPES, 100 μM $CaCl_2$, pH 7.4 for sdFLIC experiments).

Plasmids and shRNA constructs

Plasmids and shRNA constructs used for preparations of DCVs have been previously described (20). For simultaneous shRNA knockdown of multiple syt isoforms, a modified pLKO.5 vector containing shRNA expression cassettes targeting syt1 (TRCN0000093258) and syt9 (TRCN0000379591) from Mission shRNA plasmids (Sigma-Aldrich) was used.

Cell culture

Wild-type pheochromocytoma cells (PC12) and a PC12 cell line stably expressing a syt1-syt9 double knock-down shRNA cassette were cultured as previously described (20) on 10 cm plastic cell culture plates at 37ºC in 10% CO_2 in Dulbecco's Modified Eagle Medium (DMEM) High Glucose 1 X Gibco supplemented with 10% horse serum (Cellgro), 10% calf serum (Fe^+) (Hyclone), and 1% penicillin/streptomycin mix. Medium was changed every 2-3 days and cells were passaged after reaching 90% confluency by incubating 5 min in HBSS and re-plating in fresh medium. Cells were transfected with NPY-Ruby by electroporation using an Electro Square Porator ECM 830 (BTX). After harvesting and sedimentation, cells were suspended in a small volume of sterile cytomix electroporation buffer[58] (120 mM KCl, 10 mM KH_2PO_4, 0.15 mM $CaCl_2$, 2 mM EGTA, 25 mM HEPES-KOH, 5 mM $MgCl_2$, 2 mM ATP, and 5 mM glutathione, pH 7.6) and then counted and diluted to ~14 x 10^6 cells/mL. 700 μL of cell suspension (~10x10^6 cells) and 30 μg of DNA were placed in an electroporator cuvette with 4 mm gap and two 255V, 8 ms electroporation pulses were applied. Cells were then transferred to a 10 cm cell culture dish with 10 mL of normal growth medium. NPY-Ruby transfected cells were cultured under normal conditions for 3 days after transfection and then used for fractionation.

DCV purification

DCVs were purified using an iso-osmotic density gradient as previously described (20). PC12 cells (15-30 10-cm plates depending on experiments) were scraped into PBS, pelleted by centrifugation, resuspended, and washed once in homogenization medium (0.26 M sucrose, 5 mM MOPS, and 0.2 mM EDTA). Following resuspension in (3 ml) homogenization medium containing protease inhibitor (Roche Diagnostics), the cells were cracked open using a ball bearing homogenizer with a 0.2507-inch bore and 0.2496-inch diameter ball. The homogenate was then spun at 4000 rpm (1000 x g), 10 min at 4ºC in fixed-angle microcentrifuge to pellet nuclei and larger debris. The postnuclear supernatant (PNS) was collected and spun at 11,000 rpm (8000 x

g), 15 min at 4°C to pellet mitochondria. The postmitochondrial supernatant (PMS) was then collected, adjusted to 5 mM EDTA, and incubated 10 min on ice. A working solution of 50% Optiprep (iodixanol) (5 vol 60% Optiprep: 1 vol 0.26M sucrose, 30 mM MOPS, 1 mM EDTA) and homogenization medium were mixed to prepare solutions for discontinuous gradients in Beckman SW55 tubes: 0.5 mL of 30% iodixanol on the bottom and 3.8 mL of 14.5% iodixanol, above which 1.2 ml EDTA-adjusted PMS was layered. Samples were spun at 45,000 rpm (190,000 x g) for 5 h. A clear white band at the interface between the 30% iodixanol and the 14.5% iodixanol was collected as the DCV sample. The DCV sample was then extensively dialyzed (2-3 buffer changes) in a cassette with 10,000 kD molecular weight cutoff (24-48 h, 3 x 5L) into the fusion assay buffer (120 mM potassium glutamate, 20 mM potassium acetate, 20 mM HEPES, pH 7.4).

Site-directed fluorescence interference contrast (sd-FLIC) microscopy

The principle of site-directed fluorescence interference contrast (FLIC) microscopy and the set up as used in this work, has been described previously (30). A membrane containing protein with specifically labeled cysteines is supported on a patterned silicon chip with microscopic steps of silicon dioxide. The fluorescence intensity depends on the position of the dye with respect to the standing modes of the exciting and emitting light in front of the reflecting silicon surface. The position is determined by the variable-height 16 oxide steps and the constant average distance between dye and silicon oxide (35).

Images were acquired on a Zeiss Axiovert 200 or Axio Observer 7 fluorescence microscope (Carl Zeiss) with a mercury lamp as a light source and a 40× water immersion objective (Zeiss; N.A. = 0.7). Fluorescence was observed through a 610-nm band-pass filter (D610/60; Chroma) by a CCD camera (DV-887ESC-BV; Andor-Technologies). Exposure times for imaging were set between 40 and 80 ms, and the excitation light was filtered by a neutral density filter (ND 1.0, Chroma) to avoid photobleaching.

During sdFLIC experiments, we acquired 4-6 images, 20-30 min after buffer changes, for each membrane condition of one supported membrane. From each image, we extracted 100 sets of 16 fluorescence intensities and fitted the optical theory with the fluorophore-membrane distance as fit parameter. Software to fit the data was kindly provided by the authors of (35). The standard deviation of these ~400-600 results were usually in the order of 1 nm. The optical model consists of 5 layers of different thickness and refractive indices (bulk silicon, variable silicon oxide, 4 nm water, 4 nm membrane, bulk water), which we kept constant for all conditions (30, 36, 37). The reported errors for the absolute membrane distance are the standard errors from at least 3 repeats. Not included in these errors are systematic errors that might origin in different membrane thicknesses or membrane-substrate distances between different lipid conditions and a systematic underestimation of the residue-membrane distance from 10-20% of protein that is trapped on the substrate proximal side of the supported bilayer. The reported errors after buffer changes or the addition of C2AB are the standard errors of the detected distance changes from at least 3 repeats

for each condition. Based on previous experiments with polymer supported bilayers we estimate the systematic uncertainty for the measured absolute distance to be ~1-2 nm (36). Statistics for sdFLIC data may be found in Table S4.

Total internal reflection fluorescence (TIRF) microscopy

Experiments examining single-vesicle docking and fusion events were performed on a Zeiss Axiovert 35 fluorescence microscope (Carl Zeiss, Thornwood, NY), equipped with a 63x water immersion objective (Zeiss; N.A. = 0.95) and a prism-based TIRF illumination. The light source was an OBIS 532 LS laser from Coherent Inc. (Santa Clara CA). Fluorescence was observed through a 610 nm band pass filter (D610/60; Chroma, Battleboro, VT) by an electron multiplying CCD (DU-860E; Andor Technologies). The prism-quartz interface was lubricated with glycerol to allow easy translocation of the sample cell on the microscope stage. The beam was totally internally reflected at an angle of 72° from the surface normal, resulting in an evanescent wave that decays exponentially with a characteristic penetration depth of ~100 nm. An elliptical area of 250 x 65 μm was illuminated. The laser intensity, shutter, and camera were controlled by a homemade program written in LabVIEW (National Instruments, Austin, TX).

Single DCV fusion assay

Acceptor t-SNARE protein containing planar supported bilayers were washed with fusion buffer containing EDTA or divalent metal Ca^{2+} as indicated in text. They were then perfused with DCV (50-100 μL depending on preparation) diluted into 2 mL of fusion buffer (120 mM potassium glutamate, 20 mM potassium acetate, 20 mM HEPES, pH 7.4) with additions of 100 μM EDTA, or 100 μM Ca^{2+} with or without 0.4 μM C2AB as indicated in text. The fluorescence from DCVs was recorded by exciting with the 532 nm laser and using a EMCCD camera. After injection of the DCV sample, the microscope was focused within no more than 30 seconds and then a total of 5000 images were taken with 200 ms exposure times and spooled directly to the hard drive.

Single-vesicle fusion data were analyzed using a homemade program written in LabVIEW (National Instruments, Austin, TX). Stacks of images were filtered by a moving average filter. The maximum intensity for each pixel over the whole stack was projected on a single image. Vesicles were located in this image by a single-particle detection algorithm described in (38). The peak (central pixel) and mean fluorescence intensities of a 5 x 5 $pixel^2$ area around each identified center of mass were plotted as a function of time for all particles in the image series. Docking was quantified by determining the number of vesicles that bound to the surface during the 10-minute experiment after their addition to the supported membrane and normalizing relative to a standard condition.

The fusion efficiency was determined from the number of vesicles that underwent fusion within 15 s after they docked relative to the total number of vesicles that docked. The fusion kinetics was

determined by measuring the time delay between time of docking and onset of fusion for each fusing vesicle. The resulting cumulative distribution function was normalized by the fusion efficiency. Results are reported as mean ± standard errors from 5 repeats of the experiments. Release modes of individual fusion events were quantified by normalizing the peak intensity trace originating from vesicles by their intensity during the docked state. The intensity increase ΔI_C was determined from single vesicles and graphed as box-plots (center line: median, box defines upper and lower quartiles, whiskers illustrate min and max) with raw data. Statistics for single vesicle fusion data may be found in Tables S5 and S6.

References

1. R. Jahn, R. H. Scheller, SNAREs--engines for membrane fusion. *Nature reviews. Molecular cell biology* **7**, 631-643 (2006).
2. R. Jahn, D. Fasshauer, Molecular machines governing exocytosis of synaptic vesicles. *Nature* **490**, 201-207 (2012).
3. J. Rizo, T. C. Sudhof, The membrane fusion enigma: SNAREs, Sec1/Munc18 proteins, and their accomplices--guilty as charged? *Annu Rev Cell Dev Biol* **28**, 279-308 (2012).
4. E. R. Chapman, How does synaptotagmin trigger neurotransmitter release? *Annu Rev Biochem* **77**, 615-641 (2008).
5. J. Bai, W. C. Tucker, E. R. Chapman, PIP2 increases the speed of response of synaptotagmin and steers its membrane-penetration activity toward the plasma membrane. *Nat Struct Mol Biol* **11**, 36-44 (2004).
6. D. Z. Herrick, S. Sterbling, K. A. Rasch, A. Hinderliter, D. S. Cafiso, Position of synaptotagmin I at the membrane interface: cooperative interactions of tandem C2 domains. *Biochemistry* **45**, 9668-9674 (2006).
7. W. Kuo, D. Z. Herrick, J. F. Ellena, D. S. Cafiso, The calcium-dependent and calcium-independent membrane binding of synaptotagmin 1: two modes of C2B binding. *J Mol Biol* **387**, 284-294 (2009).
8. A. Perez-Lara *et al.*, PtdInsP2 and PtdSer cooperate to trap synaptotagmin-1 to the plasma membrane in the presence of calcium. *Elife* **5** (2016).
9. Q. Zhou *et al.*, Architecture of the synaptotagmin-SNARE machinery for neuronal exocytosis. *Nature* **525**, 62-67 (2015).
10. Q. Zhou *et al.*, The primed SNARE-complexin-synaptotagmin complex for neuronal exocytosis. *Nature* **548**, 420-425 (2017).
11. Y. Park *et al.*, Synaptotagmin-1 binds to PIP(2)-containing membrane but not to SNAREs at physiological ionic strength. *Nat Struct Mol Biol* **22**, 815-823 (2015).
12. V. Kiessling *et al.*, A molecular mechanism for calcium-mediated synaptotagmin-triggered exocytosis. *Nat Struct Mol Biol* **25**, 911-917 (2018).
13. C. C. Lin *et al.*, Control of membrane gaps by synaptotagmin-Ca2+ measured with a novel membrane distance ruler. *Nat Commun* **5**, 5859 (2014).
14. S. B. Nyenhuis, A. Thapa, D. S. Cafiso, Phosphatidylinositol 4,5 Bisphosphate Controls the cis and trans Interactions of Synaptotagmin 1. *Biophys J* **117**, 247-257 (2019).
15. A. L. Lai, L. K. Tamm, J. F. Ellena, D. S. Cafiso, Synaptotagmin 1 modulates lipid acyl chain order in lipid bilayers by demixing phosphatidylserine. *J Biol Chem* **286**, 25291-25300 (2011).
16. M. Xue, C. Ma, T. K. Craig, C. Rosenmund, J. Rizo, The Janus-faced nature of the C(2)B domain is fundamental for synaptotagmin-1 function. *Nat Struct Mol Biol* **15**, 1160-1168 (2008).
17. D. Z. Herrick *et al.*, Solution and membrane-bound conformations of the tandem C2A and C2B domains of synaptotagmin 1: Evidence for bilayer bridging. *J Mol Biol* **390**, 913-923 (2009).
18. G. Jeschke, MMM: A toolbox for integrative structure modeling. *Protein Sci* **27**, 76-85 (2018).
19. A. J. B. Kreutzberger *et al.*, In vitro fusion of single synaptic and dense core vesicles reproduces key physiological properties. *Nat Commun* **10**, 3904 (2019).

20. A. J. B. Kreutzberger *et al.*, Reconstitution of calcium-mediated exocytosis of dense-core vesicles. *Sci Adv* **3**, e1603208 (2017).
21. A. J. B. Kreutzberger *et al.*, Asymmetric Phosphatidylethanolamine Distribution Controls Fusion Pore Lifetime and Probability. *Biophys J* **113**, 1912-1915 (2017).
22. A. C. Wolfes, C. Dean, The diversity of synaptotagmin isoforms. *Curr Opin Neurobiol* **63**, 198-209 (2020).
23. M. Bendahmane *et al.*, Synaptotagmin-7 enhances calcium-sensing of chromaffin cell granules and slows discharge of granule cargos. *J Neurochem* 10.1111/jnc.14986 (2020).
24. H. I. Ingolfsson *et al.*, Computational Lipidomics of the Neuronal Plasma Membrane. *Biophys J* **113**, 2271-2280 (2017).
25. L. K. Tamm, J. Crane, V. Kiessling, Membrane fusion: a structural perspective on the interplay of lipids and proteins. *Curr Opin Struct Biol* **13**, 453-466 (2003).
26. H. S. Hendrickson, Physical properties and interactions of phosphoinositides. *Ann N Y Acad Sci* **165**, 668-676 (1969).
27. P. A. Janmey, K. Iida, H. L. Yin, T. P. Stossel, Polyphosphoinositide micelles and polyphosphoinositide-containing vesicles dissociate endogenous gelsolin-actin complexes and promote actin assembly from the fast-growing end of actin filaments blocked by gelsolin. *J Biol Chem* **262**, 12228-12236 (1987).
28. R. Zdanowicz *et al.*, Complexin Binding to Membranes and Acceptor t-SNAREs Explains Its Clamping Effect on Fusion. *Biophys J* **113**, 1235-1250 (2017).
29. A. A. Frazier, C. R. Roller, J. J. Havelka, A. Hinderliter, D. S. Cafiso, Membrane-bound orientation and position of the synaptotagmin I C2A domain by site-directed spin labeling. *Biochemistry* **42**, 96-105 (2003).
30. B. Liang, V. Kiessling, L. K. Tamm, Prefusion structure of syntaxin-1A suggests pathway for folding into neuronal trans-SNARE complex fusion intermediate. *Proc Natl Acad Sci U S A* **110**, 19384-19389 (2013).
31. M. K. Domanska, V. Kiessling, A. Stein, D. Fasshauer, L. K. Tamm, Single vesicle millisecond fusion kinetics reveals number of SNARE complexes optimal for fast SNARE-mediated membrane fusion. *J Biol Chem* **284**, 32158-32166 (2009).
32. E. Kalb, S. Frey, L. K. Tamm, Formation of supported planar bilayers by fusion of vesicles to supported phospholipid monolayers. *Biochim Biophys Acta* **1103**, 307-316 (1992).
33. M. L. Wagner, L. K. Tamm, Tethered polymer-supported planar lipid bilayers for reconstitution of integral membrane proteins: silane-polyethyleneglycol-lipid as a cushion and covalent linker. *Biophys J* **79**, 1400-1414 (2000).
34. M. L. Wagner, L. K. Tamm, Reconstituted syntaxin1a/SNAP25 interacts with negatively charged lipids as measured by lateral diffusion in planar supported bilayers. *Biophys J* **81**, 266-275 (2001).
35. A. Lambacher, P. Fromherz, Luminescence of dye molecules on oxidized silicon and fluorescence interference contrast microscopy of biomembranes. *J. Opt. Soc. Am. B* **19**, 1435-1453 (2002).
36. J. M. Crane, V. Kiessling, L. K. Tamm, Measuring lipid asymmetry in planar supported bilayers by fluorescence interference contrast microscopy. *Langmuir* **21**, 1377-1388 (2005).
37. V. Kiessling, L. K. Tamm, Measuring distances in supported bilayers by fluorescence interference-contrast microscopy: polymer supports and SNARE proteins. *Biophys J* **84**, 408-418 (2003).

38. V. Kiessling, J. M. Crane, L. K. Tamm, Transbilayer effects of raft-like lipid domains in asymmetric planar bilayers measured by single molecule tracking. *Biophys J* **91**, 3313-3326 (2006).

Acknowledgements: This work was supported by NIH grant NIGMS GM072694 to LKT and DSC. We would like to thank Dr. David A. Nyenhuis for providing software for the routine phasing and normalization of the EPR spectra.

Author contributions: S.B.N and N.K. designed the EPR experiments, expressed and labeled Syt1, performed power saturation and EPR measurements on Syt1 C2AB and analyzed the data. V.K. and A.K. designed and performed single particle fusion assays on Syt1 C2AB and its mutants and analyzed the data. V.K. designed and performed FLIC data on SNARE proteins. B.L. expressed, isolated and reconstituted membrane associated SNAREs. A.T. performed membrane binding measurements on C2AB and carried out initial EPR power saturation measurements on C2AB mutants. L.K.T and D.S.C. designed the experiments and analyzed the data. S.B.N., V.K., A. K. B.L., L.K.T. and D.S.C. wrote the manuscript.

Competing interests: The authors declare no financial interests in the outcome of this study.

Data availability:
Data is available on request from either V.K. (single event fusion or fluorescence data) or D.S.C. (EPR data).

Code availability:
Code that was used for the processing of EPR data is available from D.S.C. upon request.